AN ICE FLOW MODEL AND ITS APPLICATION TO A FLOWLINE IN THE CENTRAL PORTION OF THE GREENLAND ICE SHEET

by
Cynthia A. Richardson

Senior Thesis
Presented in partial fulfillment
of the requirements for
the degree of
Bachelor of Science
in the
Department of Geology and Mineralogy
The Ohio State University

Spring, 1980.

approved

Dr. Ian M. Whillans,
advisor

ABSTRACT. Radar soundings from Greenland show internal layering in the ice sheet. Many investigators have suggested that these layers represent ancient depositional surfaces.

An ice flow model assuming steady-state is used to calculate depths of isochrons. This model uses measured ice thickness and accumulation rates to calculate vertical and horizontal velocities. From this vertical strain rates, average annual layer thickness, and depths of isochrons are calculated.

Comparison of the calculated isochrons with the internal radar layering shows close agreement between shallow-depth radar layering and young isochrons, but increasing discrepancies with depth. This is interpreted as showing that the layers do represent isochrons, but that the steady-state assumption used in the model is not valid for calculating older and deeper layers.

Decreasing thickness and accumulation values brings closer agreement to lower, older layers, indicating that the ice sheet has not been in a steady-state in the past and that thickness and accumulation were probably smaller in the past and have increased to present-day values.

ACKNOWLEDGEMENTS

I wish to extend my heartfelt appreciation to the following people: Dr. Colin Bull and Dr. Leslie Blatt, for serving on my thesis committee and offering helpful suggestions and food for thought; Mr. Søren Overgaard, for providing radar data and information; Barb Richardson, for dictating miles of numbers over the phone when data got left in the wrong place; Richard Alley for lots of moral support and a firm shove whenever I slowed doww too much, and most of all, Dr. Ian Whillans, my thesis advisor, for his constant advice, encouragemnt, and prodding, and for the hours he spent helping me try to understand this material. Without these people, this thesis would never have been completed.

TABLE OF CONTENTS

INTRODUCTION

High frequency airborne radio echo sounding methods were originally developed to study the thickness of a glacier. When used on ice sheets, additional, unexpected results were obtained. Not only were surface and substrate echoes recorded on the radar photographs, but internal layering appeared as well (see figure 1).

A number of hypotheses concerning the causes of the internal layering have been advanced. Harrison (1973) proposed that the echoes were a result of varying orientations of anisotropic ice crystals. Robin (1969) suggested that a change from bubbly ice to clear ice caused a change in permittivity which resulted in varying amplitudes of the reflections causing the layering. Clough (1977) suggested the theory that changes in the density of the ice caused changes in the reflections of the electromagnetic pulse resulting in the phenomenon. The above authors, and others, all considered the possibility that the radio reflections come from ancient depositional layers of some kind. It is now generally accepted that the reflecting layers probably are ancient depositional layers (Clough, 1977), although the

Figure 1. Radar record photograph. CBD no. 230 (left side of picture) is about 80 kilometers from the ice divide. Arrows indicate internal layers used in this study.

FLIGHT 0578
60 MHZ 1.17

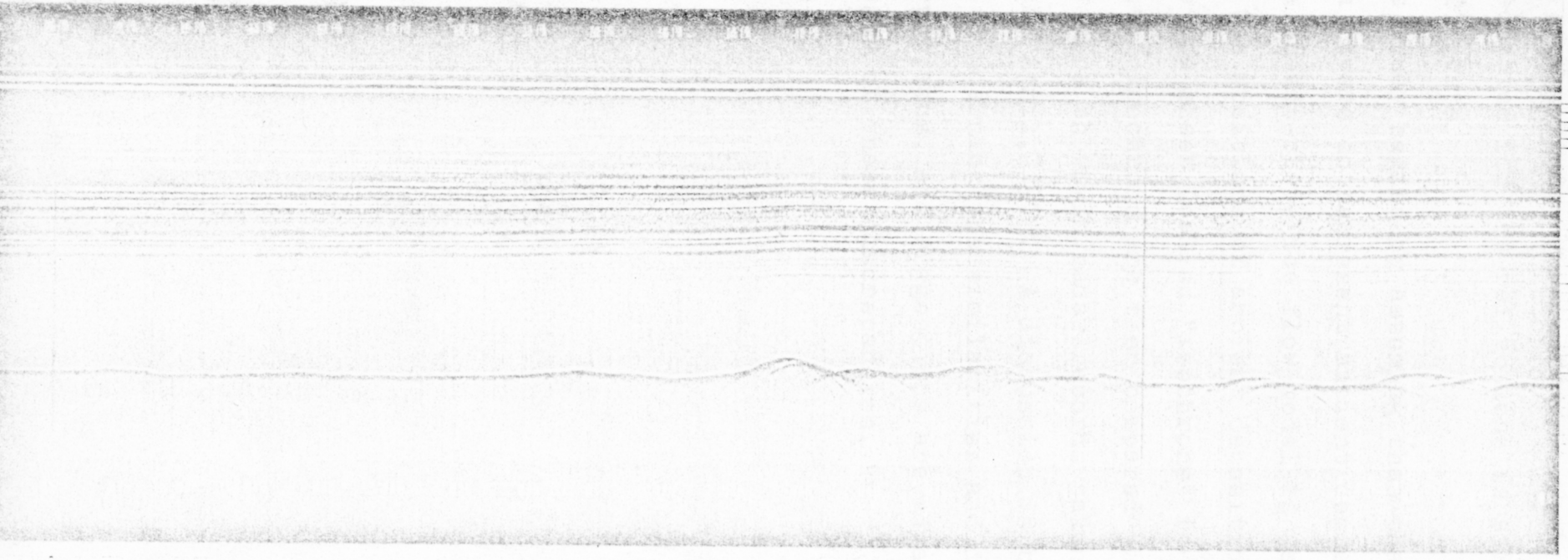

230 240 250

precise mechanism for the reflections is still a subject of debate.

This study begins by assuming that the internal reflection layers do represent ancient depositional layers. A steady-state ice flow model is used to calculate the positions of ancient depositional layers within the ice sheet (called "isochrons" in this study). These isochrons are then compared to the internal layers shown in radar records taken in Greenland in April, 1978. A discussion is then presented, concerning the similarities and discrepancies of the comparisons, and suggestions are advanced as to the causes of these discrepancies.

DATA

Ice thickness and internal reflection layer depth data of part of the Greenland ice sheet were obtained from radio echo sounding records of flight 0578 of April, 1978. These records were provided by Mr. Søren Overgaard of the Electromagnetic Institute of the Technical University of Denmark. The flight path is shown in figure 2.

The records were supplied as strips of photographic film on which radio reflections from the air-ice surface, subglacial surface and internal reflecting layers appear as white lines (figure 1). Four white lines are visible at the top of each record, the first not as well defined as the other three. The second line down represents the aircraft, while the fourth line down is the air-ice surface (Overgaard, written communication to I. M. Whillans, 1979). The subglacial surface is the lowermost reflection. Internal reflections occur throughout the thickness of the ice, but are clearly visible only in the upper three-fourths of the ice.

At the top and bottom of the record, identification numbers, called CBD numbers are printed. These numbers are used to collate the photographs with a

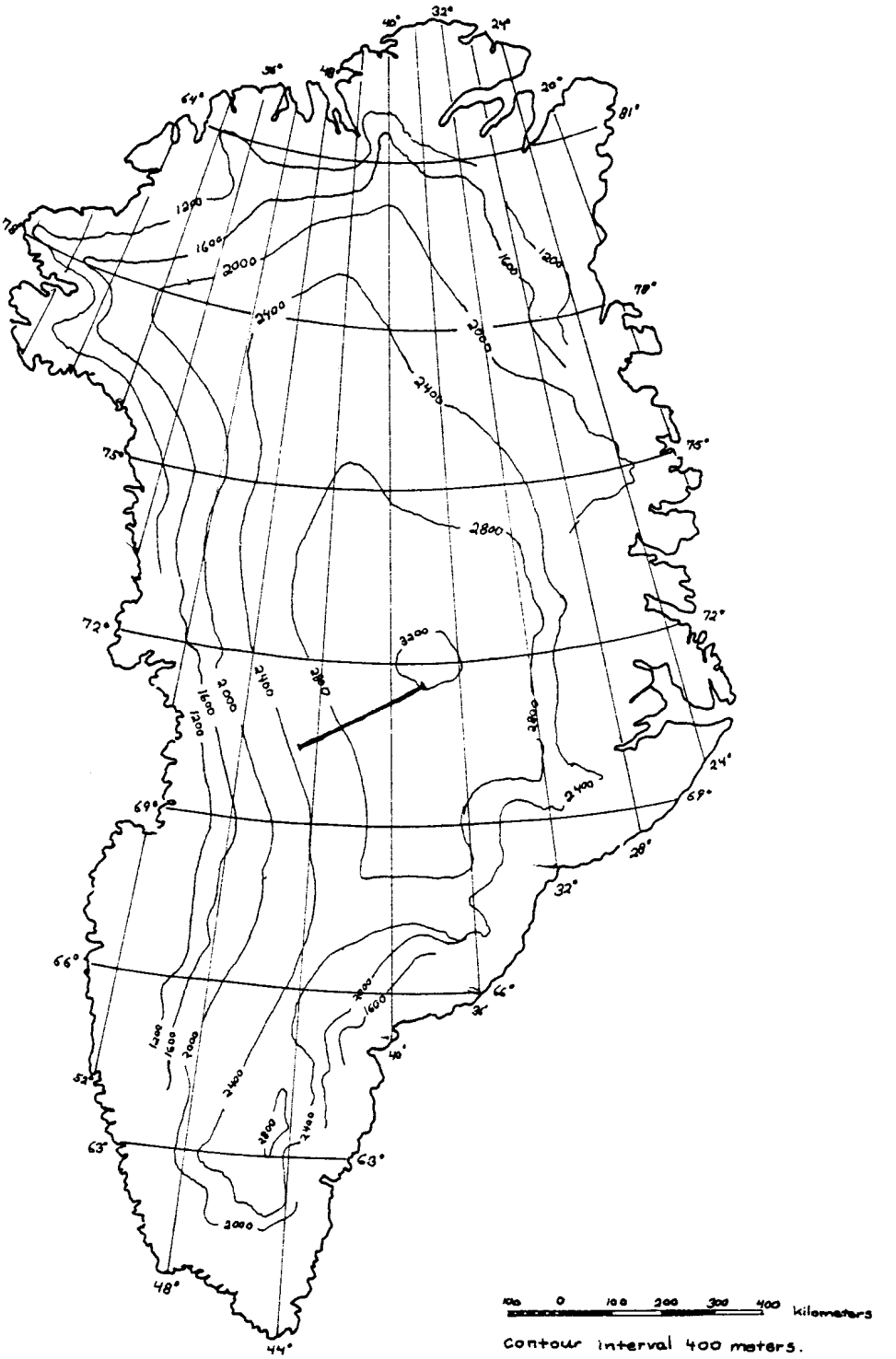

Figure 2. Map of Greenland showing flight path of flight 0578. Flight path is indicated by bold line in central Greenland.

computer-printout of latitude, longitude and air-ice surface elevation. Aircraft altitude and groundspeed, and the time of the pulse are also recorded at each CBD number, but were not necessary for this study.

The depths of three internal reflections were measured for comparison with calculated isochrons. Lines were selected that were bright, continuous, and evenly spaced through the region of clear internal reflections. A scale, provided by Mr. Overgaard for use specifically with these records, was used to obtain ice thickness and the depths of internal reflections. Measurements were taken from the bottom of the line representing the air-ice surface to the bottom of the reflection being measured. The scale was calibrated in hundreds of meters and read to the nearest ten meters.

Elevations of the measured lines were obtained by subtracting measured depths from the surface elevations provided on the computer-printout. The substrate and air-ice surface elevations were compared to independently generated contour maps of Greenland (Benson, 1962; Weidick, 1975) and found to

agree within about 5% vertically.

Accumulation data are from Benson (1962). Benson presented a contour map of gross accumulation rates in centimeters of water per year . This map incorporates all of the data available to Benson at that time. It was decided that this map should be used for obtaining accumulation rates, because by incorporating numerous studies, errors arising from a single study or from an abnormal year can be avoided.

The accumulation map was enlarged and the flight path was plotted on it. Accumulation rates were calculated for each CBD number along the flowline using an interpolation of the accumulation data (see figure 3). Although this map contains gross annual accumulation rates, these rates can be considered as approximate to net accumulation rates. This is because the flight path does not extend into the ablation or saturation facies, which are located on the outer edges of Greenland (Benson, 1962). In the inland facies, sublimation is not a significant factor, so that net rates approximately equal gross accumulation rates. Accumulation rates in centimeters of water per year calculated for the CBD numbers were converted to meters of ice

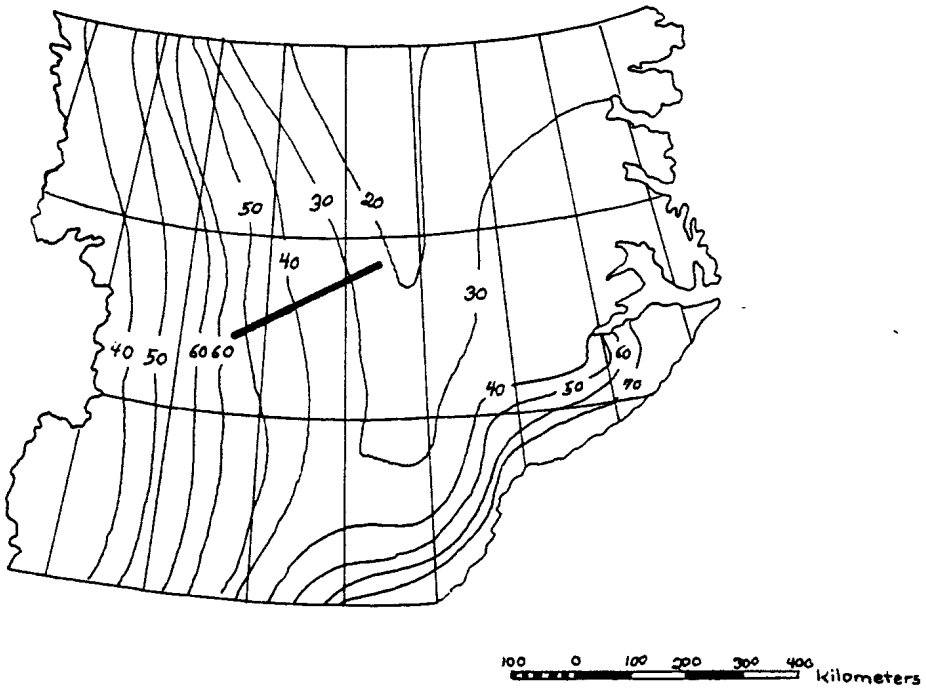

Figure 3.
Map of Greenland showing part of Benson's (1962) accumulation data. Contours are in cm H_2O/a. Flight path is indicated by bold line.

per year by dividing by a density factor of 92 cm H_2O / m ice.

The distances from the ice divide assigned to each CBD number were measured by plotting the flight path on a large (1:2,500,000) map of Greenland (Weidick, 1975), measuring the distance along the flowline, and converting according to the scale of the map. The distances were measured to the nearest kilometer.

THE MODEL

A version of the ice flow model developed by I.M. Whillans (1976) is used to calculate isochrons. This model assumes that the ice is in a steady-state (thickness and velocity at a given point on the ice sheet do not change with time), that vertical strain rates are constant with depth, but can vary laterally, and that there is no bottom melting or freezing. These assumptions are discussed in the sections concerning results and interpretations.

Flow in an ice sheet is along the surface elevation gradient (Paterson, 1969). Radar data, showing internal layering of the inland ice, were collected along the flight path shown in figure 2. This path is roughly perpendicular to the surface elevation contours, and is therefore considered a flowline. For a considerable distance north and south of this flowline, the neighboring flowlines are approximately parallel. Therefore, the flow pattern in the area of this study is largely two-dimensional.

In this model, equations for horizontal and vertical velocities are derived. From these equations, vertical strain rates, average layer

thickness and, ultimately, the depth of a selected isochron at any given point can be calculated. This section describes the model and shows how these values are derived.

Consider a profile of an ice sheet (figure 4). In order to maintain a constant thickness, as snow accumulates upglacier, there is an equivalent flow away from the ice divide. Thus, the accumulation of snow upglacier ($\dot{b}$) summed along the flowline ($\Sigma \dot{b} \Delta x$, where x is the horizontal distance) is equal to the product of the average horizontal velocity ($\bar{U}$) and the thickness of the ice sheet (z) at the place of measurement. Horizontal velocity decreases with depth (Paterson, 1969). However, in this model, an average horizontal velocity, taken through the thickness of the ice, is used so that:

$$\bar{U} = \frac{\Sigma \dot{b} \Delta x}{z} \qquad (1)$$

This formula is used to estimate the horizontal velocity at each CBD number along the flowline.

The vertical velocity at the ice surface is the sum of two components. In a steady-state, a particle originating at the surface moves down due to accumulation ($-\dot{b}$) and due to the vertical component of downslope movement (see figure 5).

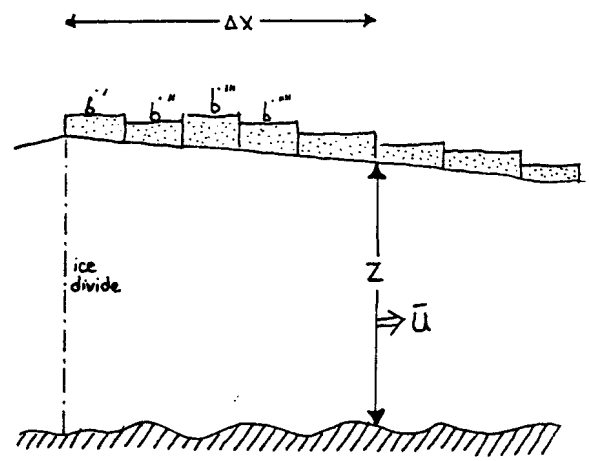

$$\bar{u}Z = \Delta x \sum \dot{b}$$

$$\bar{U} = \frac{\Delta x \sum \dot{b}}{Z}$$

Figure 4. Calculation of horizontal velocity using ice thickness, accumulation, and distance from the ice divide.

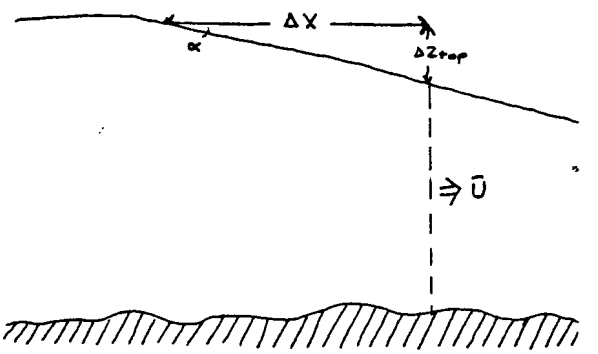

$$\tan\alpha = \frac{dz_{top}}{dx}$$

$$\text{Vertical Velocity (top)} = V_{top} = \frac{dz_{top}}{dx}\,\bar{u}$$

Figure 5. Calculation of vertical velocity at the surface of the ice sheet using change in thickness, change in distance, and horizontal velocity.

If the angle of the slope is α then tan α equals the change in elevation (dz_{top}) divided by the change in distance (dx). Multiplying by the rate of change in distance ($\bar{U}$) yields the vertical component of downslope movement associated with downslope flow. Adding the two components, the vertical velocity at the surface is:

$$v_{top} = -\dot{b} + \bar{U}\frac{dz_{top}}{dx} \qquad (2a)$$

The vertical velocity of the ice at the base of the ice sheet (v_{bot}) is no longer affected by surface accumulation. However, it is affected by the vertical component associated with downslope flow, and by a factor representing bottom freezing ($\dot{f}$). If melting occurs, $\dot{f}$ is negative. Initially, $\dot{f}$ is taken as zero. This will be discussed further in the following section. Addition of these two components yields the vertical velocity at the base of the ice:

$$v_{bot} = \dot{f} + \bar{U}\frac{dz_{bot}}{dx} \qquad (2b)$$

The vertical strain rate ($\bar{\dot{\epsilon}}_{zz}$) is defined as the rate of change of vertical velocity with depth ($\frac{dv}{dz}$). For this study, $\bar{\dot{\epsilon}}_{zz}$ is taken as constant

throughout the ice thickness. Thus:

$$\Delta V = V_{top} - V_{bot}$$

$$\Delta Z = z_{top} - z_{bot}$$

and $$\dot{\bar{\epsilon}}_{zz} = \frac{V_{top} - V_{bot}}{z_{top} - z_{bot}}$$

However $z_{top} - z_{bot}$ is equal to the ice thickness (z), so that substituting from equation 2:

$$\dot{\bar{\epsilon}}_{zz} = \frac{\left(-\dot{b} + \bar{U}\frac{dz_{top}}{dX} - \left[\dot{f} + \bar{U}\frac{dz_{bot}}{dX}\right]\right)}{z}$$

$$= \frac{-\dot{b} - \dot{f}}{z} + \frac{\bar{U}}{z}\frac{dz_{top} - dz_{bot}}{dX}$$

$$= \frac{\dot{b} - \dot{f}}{z} + \frac{\bar{U}}{z}\frac{dz}{dX} \qquad (3)$$

Layer thicknesses can now be determined. Let λ represent the thickness of a layer deposited over unit time (t). When t=0, $\lambda = \dot{b}$. Because vertical velocity varies with depth, λ varies with depth. This change in layer thickness ($d\lambda$) is described by:

$$d\lambda = \dot{\bar{\epsilon}}_{zz}\,\lambda\,dt$$

$$\int d\lambda = \int \dot{\bar{\epsilon}}_{zz}\,\lambda\,dt$$

The integral is taken from $t=t_i$ to $t=t_{i+1}$ with $t_i < t_{i+1}$. At $t=t_i$, $\lambda = \lambda_i$ and at $t=_{i+1}$,

$\lambda = \lambda_{i+1}$. The interval between t_i and t_{i+1}. Must be small enough that $\dot{\bar{\epsilon}}_{zz}$ can be considered constant. Thus:

$$\int_{\lambda_i}^{\lambda_{i+1}} \frac{d\lambda}{\lambda} = \dot{\bar{\epsilon}}_{zz} \int_{t_i}^{t_{i+1}} dt$$

$$\ln \frac{\lambda_{i+1}}{\lambda_i} = \dot{\bar{\epsilon}}_{zz} (t_{i+1} - t_i)$$

$$\lambda_{i+1} = \lambda_i \exp\left(\dot{\bar{\epsilon}}_{zz}(t_{i+1} - t_i)\right) \qquad (4)$$

If $t_i = 0$, then $\lambda_i = \dot{b}$:

$$\lambda_{i+1} = \dot{b} \exp\left(\dot{\bar{\epsilon}}_{zz}\, t_{i+1}\right) \qquad (5)$$

From this, an average thickness for an annual layer at any given location can now be calculated. A layer t_i years old is buried under t_i annual layers, so that an average layer thickness equals:

$$\bar{\lambda} = \frac{\int_{t_o}^{t_i} \lambda\, dt}{t}$$

$$= \frac{1}{t_i} \int_{t_o}^{t_i} \dot{b} \exp\left(\dot{\bar{\epsilon}}_{zz}\, t\right)$$

which was obtained by substituting from equation 5. Both $\dot{\bar{\epsilon}}_{zz}$ and $\dot{b}$ are assumed to be constant from t_o to t_i:

$$\bar{\lambda} = \frac{\dot{b}}{t_i}\int_{t_o}^{t_i} \exp\left(\bar{\dot{\epsilon}}_{zz}\, t\right) dt$$

$$= \frac{\dot{b}}{t_i\, \bar{\dot{\epsilon}}_{zz}} \left(\exp\left(\bar{\dot{\epsilon}}_{zz}\, t\right)\right)\Big|_{t_o}^{t_i}$$

$$= \frac{\dot{b}}{t_i\, \bar{\dot{\epsilon}}_{zz}} \left(\exp\left(\bar{\dot{\epsilon}}_{zz}\, t_i\right) - 1\right)$$

This is the average layer thickness over the time interval from deposition (t_o) to t_i years. Subsequent changes in layer thickness can be calculated using equation 4 with $\lambda_i = \bar{\lambda}$ and λ_{i+1} equal to the altered average thickness.

In order for the model to approximate reality, the intervals from t_o to t_i and each subsequent time step must be small enough to be able to treat $\bar{\dot{\epsilon}}_{zz}$ and $\dot{b}$ as constants across the interval. In this study, the intervals between adjacent CBD numbers were considered small enough. Using half of this interval creates a change in the average layer thickness of up to 5%, but this does not significantly alter isochron depths. The intervals between CBD numbers are referred to as "segments", with the CBD number which terminates the segment referred to as the "terminating gate", or simply "gate". Average

accumulation rate and thickness were calculated for each segment. From these, horizontal velocity and vertical strain rate were calculated for the segment. Then a time interval $(t_{i+1}-t_i)$ was calculated which is equal to the time it takes a particle to cross that segment.

An average layer thickness is calculated at each gate for all the layers originating in that segment (see figure 6). The depth of a layer deposited at the upglacier edge of segment i is:

$$\text{depth} = \bar{\lambda}_i t_i$$

in which t_i is equal to the time it takes to cross that segment. As these layers are buried further, they move horizontally into segment i+1. The average thickness of the original layers is altered by the strain rate of this new segment. These layers will also be buried under new layers originating in segment i+1. At the end of this segment, the depth of the layer which originated at the beginning of segment i is:

$$\text{depth} = \bar{\lambda}_{i+1}(t_{i+1}-t_i) + \bar{\lambda}_i t_i \exp\left(\bar{\dot{\epsilon}}_{zz_{i+1}}(t_{i+1}-t_i)\right)$$

where $(t_{i+1}-t_i)$ is the amount of time it takes to cross segment i+1, and therefore the number of annual layers deposited in that segment. This

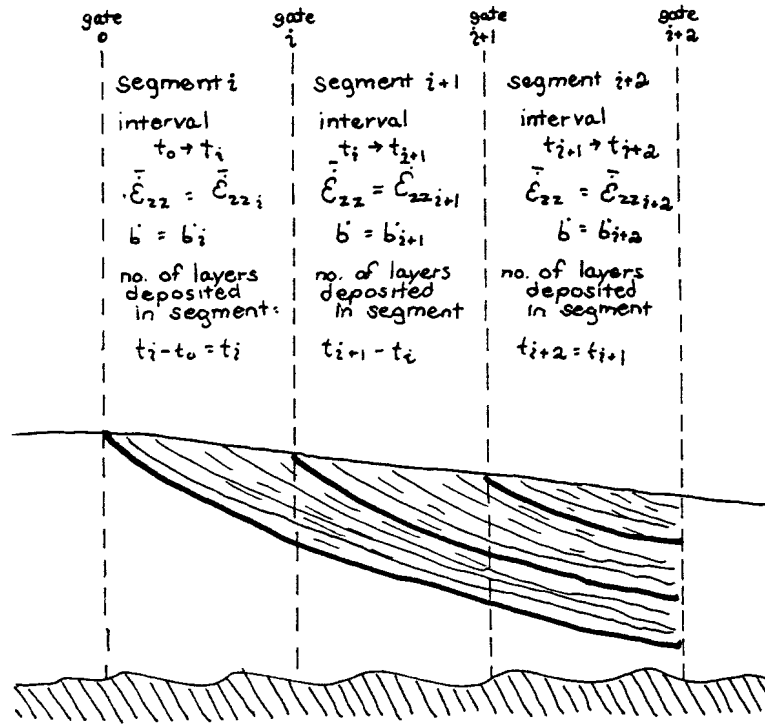

depth of bottom layer at gate i =

$$\bar{\lambda}_i t_i$$

depth of bottom layer at gate $i+1$ =

$$\lambda_{i+1}(t_{i+1} - t_i) + \bar{\lambda}_i t_i \left(\exp\left(\bar{\dot{\varepsilon}}_{zz\,i+1}(t_{i+1} - t_i)\right)\right)$$

depth of bottom layer at gate $i+2$ =

$$\lambda_{i+2}(t_{i+2} - t_{i+1}) + \Big[\lambda_{i+1}(t_{i+1} - t_i) + \lambda_i t_i \cdot \left(\exp\left(\bar{\dot{\varepsilon}}_{zz\,i+1}(t_{i+1} - t_i)\right)\right) \exp\left(\bar{\dot{\varepsilon}}_{zz\,i+2}(t_{i+2} - t_{i+1})\right)\Big]$$

Figure 6. Calculation of depth of the lower-most layer at three terminating gates.

method is continued until $t_1+t_2+t_3+\ldots=t$, with t equal to any selected age.

For this study, the depths of three layers of ages 1400, 3050, and 6700 years were determined at each CBD number along the flight path. The ages were selected to provide depths approximating the depths of the three chosen radar lines at the divide (x=0). The depths of the calculated layers were plotted and compared with the measured reflections. The results are discussed in the following sections.

RESULTS

The model described above was incorporated into a Fortran computer-program and processed on an Amdahl 470 computer to generate isochrons. Calculated isochrons were plotted using a Versatec plotter (see figure 7).

The results shown in figure 7 show close agreement between the youngest isochron and the radio reflection. This supports the contention that not only is the ice flow model valid, but that the radio reflections are indeed isochrons. This has already benn suggested by other authors (Clough, 1977; Harrison, 1973; Robin, 1969; Whillans, 1976) and is strongly supported here. Internal reflections will hereafter be referred to as isochrons in this study.

The middle and lower sets of measured and calculated isochrons do not agree as closely as the upper set. This discrepancy increases with age and depth and with increasing distance from the ice divide. The agreement at the ice divide is inherent in the model because the ages of the calculated isochrons were chosen to approximate the depths of the radar isochrons at the divide (x=0).

Figure 7. Versatec plot of the calculations showing both calculated isochrons and radar lines as measured from the radar records.

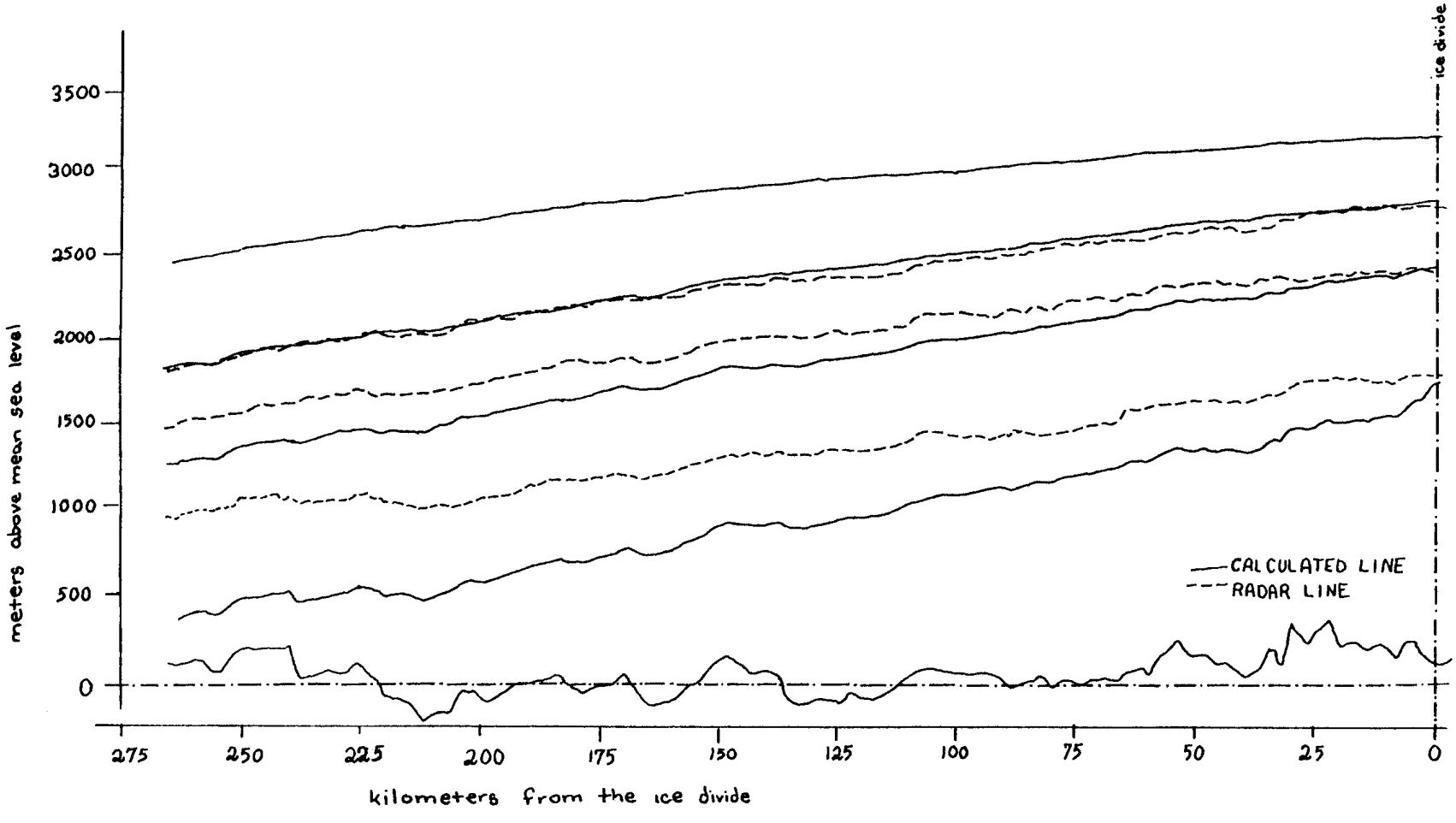
ice divide
3500
3000
2500
2000
1500
1000
500
0
meters above mean sea level
CALCULATED LINE
RADAR LINE
275
250
225
200
175
150
125
100
75
50
25
0
kilometers from the ice divide

figure 7

The calculated isochrons have to be identical to the actual isochrons at the air-ice surface. From this, it could be expected that the calculated isochrons would closely approximate the actual isochrons near the surface with the closeness of approximation decreasing with depth. This is because the data used in this study, especially accumulation and thickness measurements, apply to the present. For young, shallow isochrons, the data will be nearly correct. For isochrons of greater age, it is probable that different values of climatic parameters have affected the depositional layers. Also, minor inconsistencies in the model are amplified as calculated, simulated time passes and greater isochron depth is achieved. Therefore, one would expect to see close agreement of the calculated and observed isochrons near the surface, and less agreement with increasing depth.

This is supported by the results. The increasing differences with age may be due to three broad types of error: 1) problems with the model; 2) problems with the data; and 3) problems with climatic and internal parameters which are assumed constant, but have changed with time.

The first type of error is problems with

the model, which assumes most notably that the internal layering represents isochrons. Because the agreement of the youngest calculated and measured isochrons is too close to be coincidental, the model is considered valid. However, discrepancies between calculated and measured isochrons with depth may be due to inaccuracies of assumptions contained within the model. The model begins by assuming that vertical strain rates are constant with depth, that there is no bottom melting or freezing, and that the ice is in steady-state. Although detailed investigation of the effect of these assumptions is outside the confines of this study, some speculations can be advanced concerning the validity of these assumptions.

An increase by almost 100% in the vertical strain rates used brings close agreement to both the calculated and measured positions of the 6700 year and 3050 year old layers (see figure 8). Vertical strain rates are expected to become more nearly zero with depth (Whillans, personal communication, 1980). In this study, an average strain rate through the entire thickness of the ice is used. However, the internal layers under investigation in this study are located in only the upper 75%

Figure 8. Versatec plot showing an increase of 100% in the strain rate values used to calculate the isochrons.

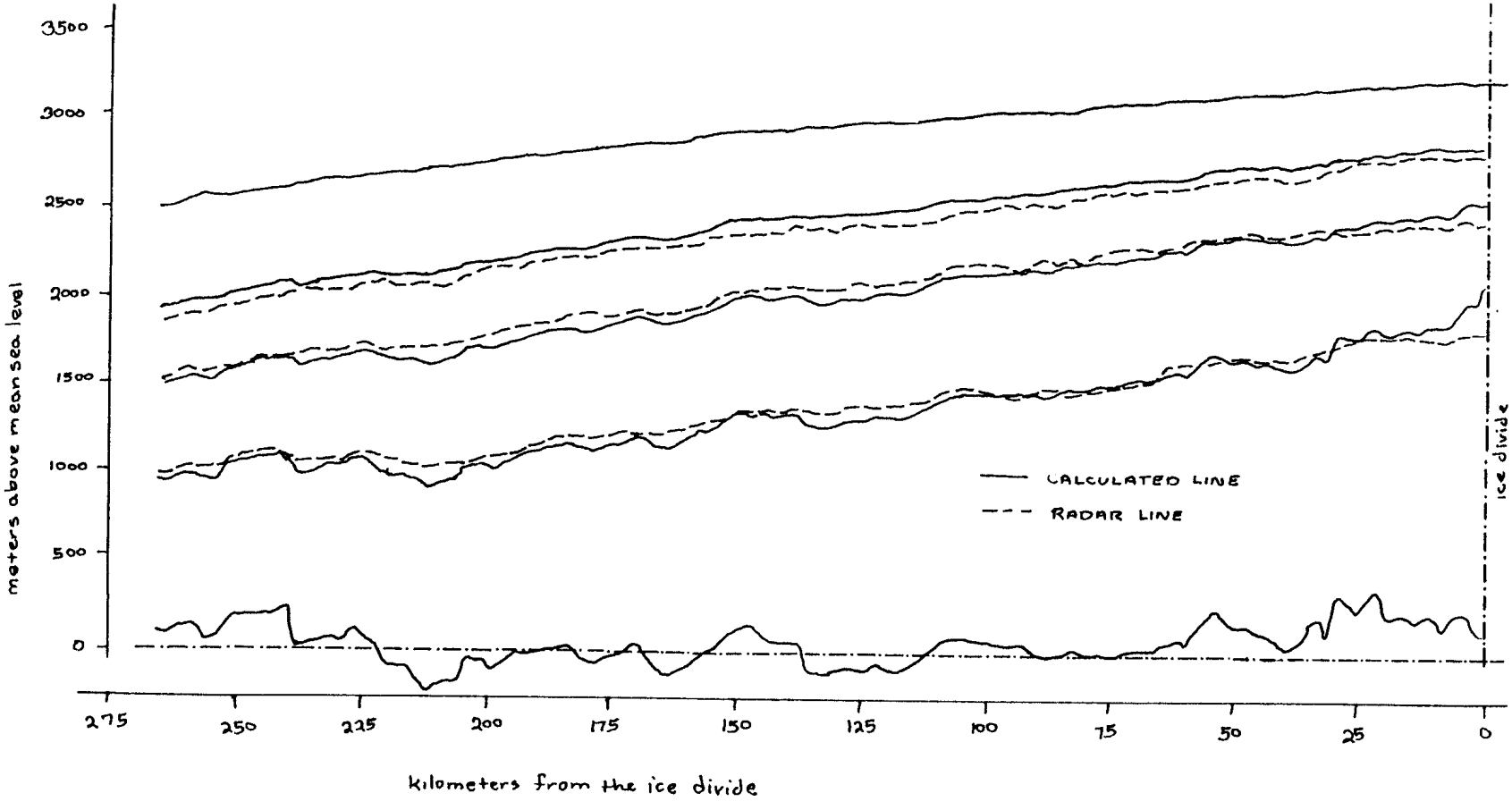
3500
3000
2500
2000
1500
1000
500
0
meters above mean sea level
CALCULATED LINE
RADAR LINE
ice divide
275
250
225
200
175
150
125
100
75
50
25
0
kilometers from the ice divide

figure 8

of the ice. Therefore, they are not directly affected by any smaller strain rates near the base of the ice. Thus a larger "average" strain rate should be used. Increasing strain rates by about 20% would be closer to what could be realistically expected. Modelling this change in the calculations resulted in little noticeable change in the calculated isochron depths. Because of this small change in depths, it is concluded that although although assuming a constant strain rate is not strictly valid, other factors have probably acted to change the radar isochron depths from those predicted by the model.

Bottom melting or freezing will affect $\dot{f}$ in equation 2b of the model:

$$V_{bot} = \dot{f} + U\frac{dz_{bot}}{dx} \qquad (2b)$$

where $\dot{f}$ was originally taken as 0. The maximum amount of melting due to geothermal heat with a standard heat flux is 0.05 cm/a and due to friction from sliding is about 0.1 cm/a/10 meters of movement (Whillans, personal communication, 1980). Along the flowline used in this study, the movement is about 30 m/a. Adding these two components together, it is seen that the maximum amount of bottom melting

is about 0.035 m/a. Substituting equation 2b into equation 3 and using $\dot{f}$ as equal to -0.035, the vertical strain rate is equal to:

$$\dot{\bar{\epsilon}} = \frac{-b}{z} + \frac{-0.035}{z} \quad \frac{\bar{U}}{z}\frac{dz}{dx} \qquad (3)$$

This changes the calculated strain rates by only about 5% which does not alter the isochron depths. Similarly, for bottom freezing, $\dot{f}$ will be positive, but of the same order of magnitude as bottom melting. This too has little effect on the calcylated isochron depths, so that bottom melting and freezing can both be neglected.

Horizontal velocity is taken as an average through the thickness. Actual values of horizontal velocity through the thickness will not normally deviate from this average value by more than 20% (Paterson, 1969). The horizontal velocities were increased and decreased by 20%, which had little effect on the calculated isochron depths. Hence, the average horizontal velocity values can be used as approximations of the actual values.

The second type of error is problems with the data. Because the air-ice and ice-substrate surface elevations agree with independently-generated maps of Greenland, these elevations are accepted as correct. This also implies the

validity of the thickness data. The radar lines are accepted as valid. The depths of these lines were measured in the same manner as the ice thickness measurements.

The only other source of data is Benson's (1962) accumulation rates. A decrease of 15% in the values of accumulation rates used will bring agreement to the middle isochrons, but will decreasethe agreement of the upper isochrons. This shows that the model is sensitive to changes in accumulation rates, and that there is no systematic error in the accumulation data.

The third and most probable type of error comes from changes in parameters assumed constant with time. These are discussed in the following section.

ALTERATIONS IN VARIABLES WITHIN THE MODEL

It has now been established that the radar lines are isochrons, that the observed data are approximately correct, and that ablation and bottom melting are insignificant along the flowline used in this study. However, there are significant differences between the older observed and calculated isochrons. The most probable explanation for these differences is variation over time of two quantities that are assumed constant with time in the model: accumulation and ice thickness. The computer-program in this study allows only calculation with constant values of ice thickness and accumulation at any location over time. Calculations were made using different values of these parameters.

A decrease in the accumulation rates used decreases the depths of the calculated isochrons. A proportional decrease in the accumulation rates has a greater effect near the margin of the ice sheet than in the interior. This is because the accumulation rates are greater at the margin. A 15% decrease in the observed accumulation rates brings approximate agreement to the 3050 year old,

or middle isochron (see figure 9), while a 30% decrease brings the lower, 6700 year old isochron to agreement (see figure 10). A decrease of 40% in the observed accumulation rates limited to the west half of the flowline brings both ends of the lower isochrons together, but discrepancies in the center of the isochrons remain (see figure 11).

All of these alterations result in a greater disagreement of the youngest, 1400 year old isochron. Because of this, any changes probably occured prior to 1400 years before present, the age of the youngest calculated isochron. The model seems to indicate that in the past the accumulation rates were less than what are observed today. These smaller rates acted over a shorter period of time (only until about 1500 years ago) than was used in the model, so that a greater magnitude of decrease in the rates may have acted in order to achieve the shallower depths obtained above.

Modelling changes in thickness yielded somewhat surprising results. A decrease of 50% in thickness values resulted in very close agreement of the 6700 year isochrons and in fairly close agreement of the 3050 year isochrons.

Figure 9. Versatec plot showing a decrease of 15% in the accumulation values used to calculate the isochrons.

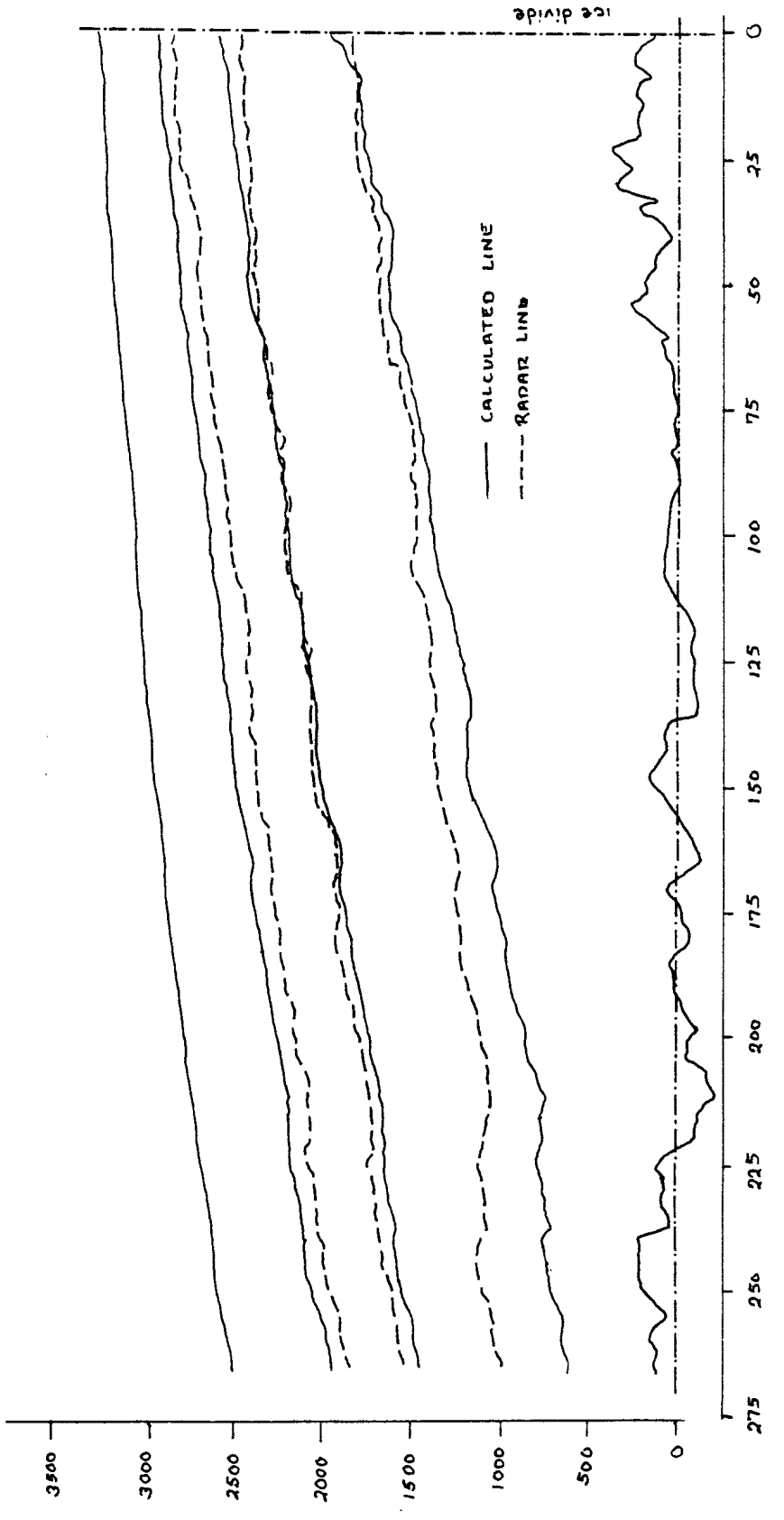
meters above mean sea level
3500
3000
2500
2000
1500
1000
500
0
ice divide
0
25
50
75
100
125
150
175
200
225
250
275
kilometers from the ice divide
CALCULATED LINE
RADAR LINE

figure 9

Figure 10. Versatec plot showing a decrease of 30% in the accumulation values used to calculate the isochrons.

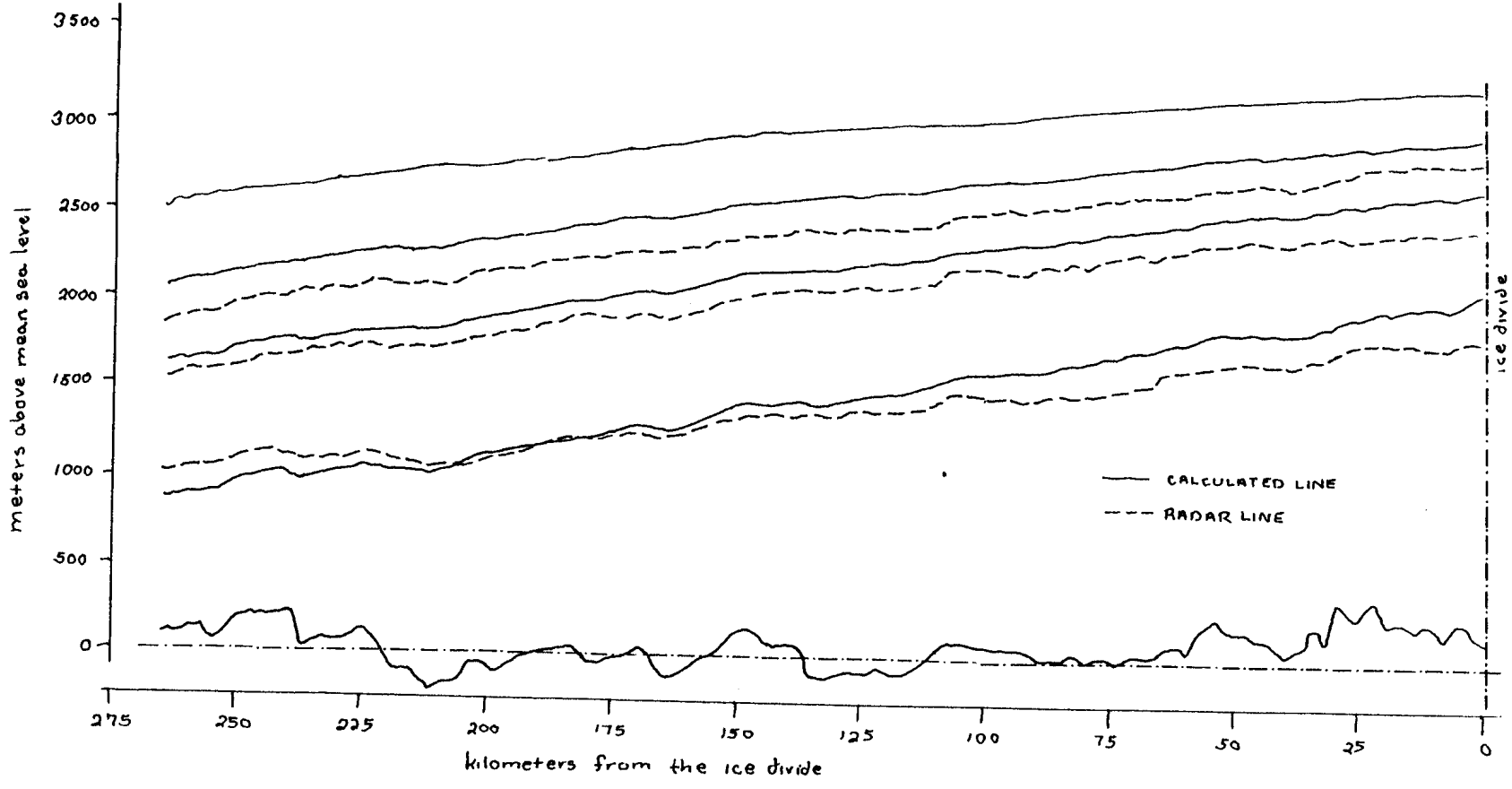
3500
3000
2500
2000
1500
1000
500
0
meters above mean sea level
CALCULATED LINE
RADAR LINE
ice divide
275
250
225
200
175
150
125
100
75
50
25
0
kilometers from the ice divide

figure 10

Figure 11. Versatec plot showing a decrease of 40% in the accumulation values on the west half of the flowline.

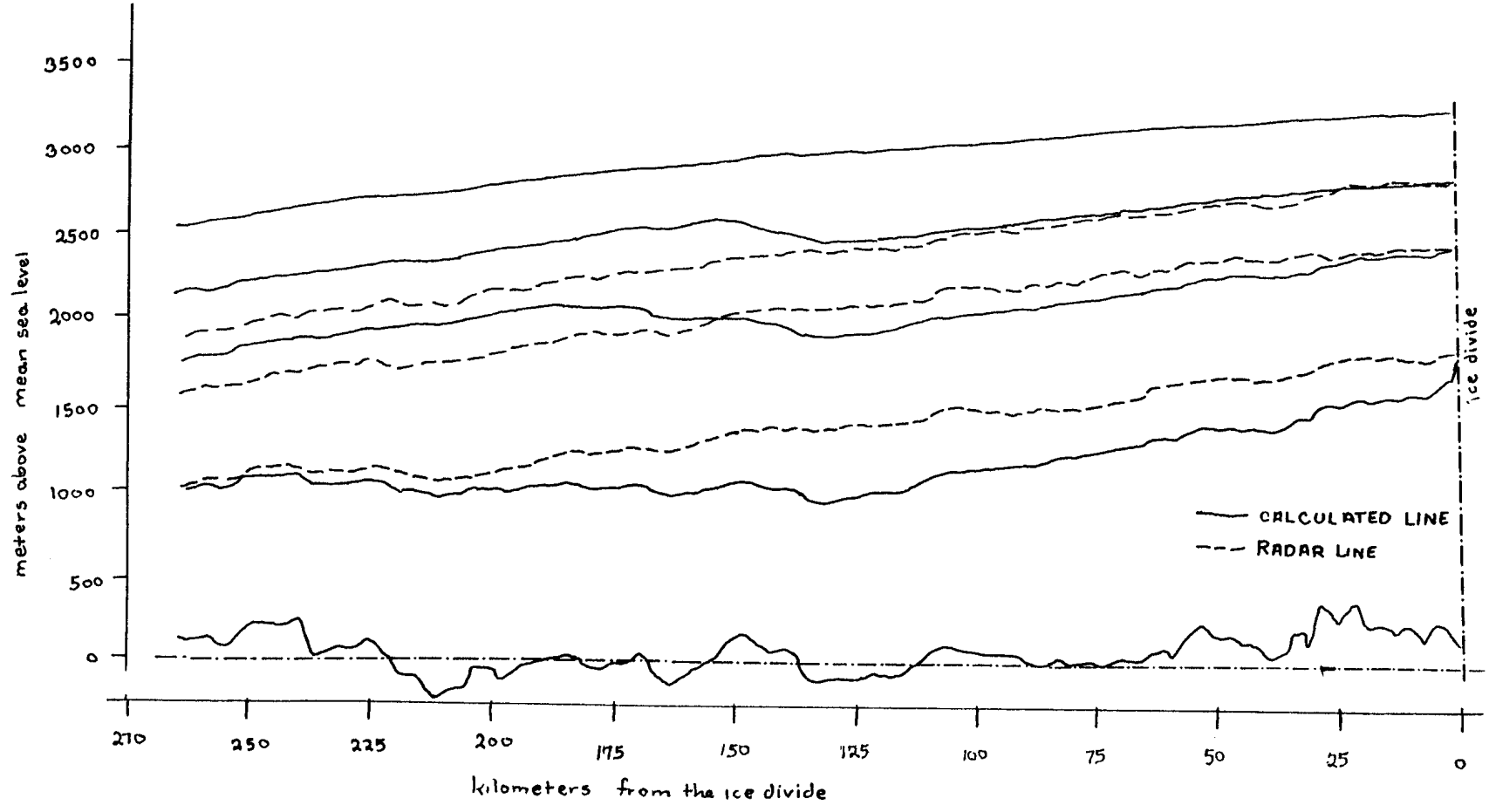
3500
3000
2500
2000
1500
1000
500
0
meters above mean sea level
CALCULATED LINE
RADAR LINE
ice divide
270
250
225
200
175
150
125
100
75
50
25
0
kilometers from the ice divide

figure 11

Again, this change decreased the agreement of the upper, 1400 year isochrons (see figure 12).

This extreme change in thickness is inconsistent with current beliefs about the mass balance of the Greenland ice sheet (Weidick, 1975). It is possible that the derivations of the model equations are wrong by an unknown factor due to variations in the ice not taken into account by the equations. The thickness values play a major role in calculation of both strain rates and horizontal velocities. The close agreement in the original model of the 1400 year old isochrons, however, suggests that there is probably not a major error in the derivation of the model.

It is conceivable that only the upper half of the ice sheet is active, and therefore only half thickness should be used in the calculations, but this seems a rather extreme interpretaition.

The most probable conclusion is that changes in accumulation and in thickness are working together, so that neither variable needs to change as much as is suggested above. From the above model, a conservative interpretaion is

Figure 12. Versatec plot showing a 50% decrease in the thickness values used to calculate the isochrons.

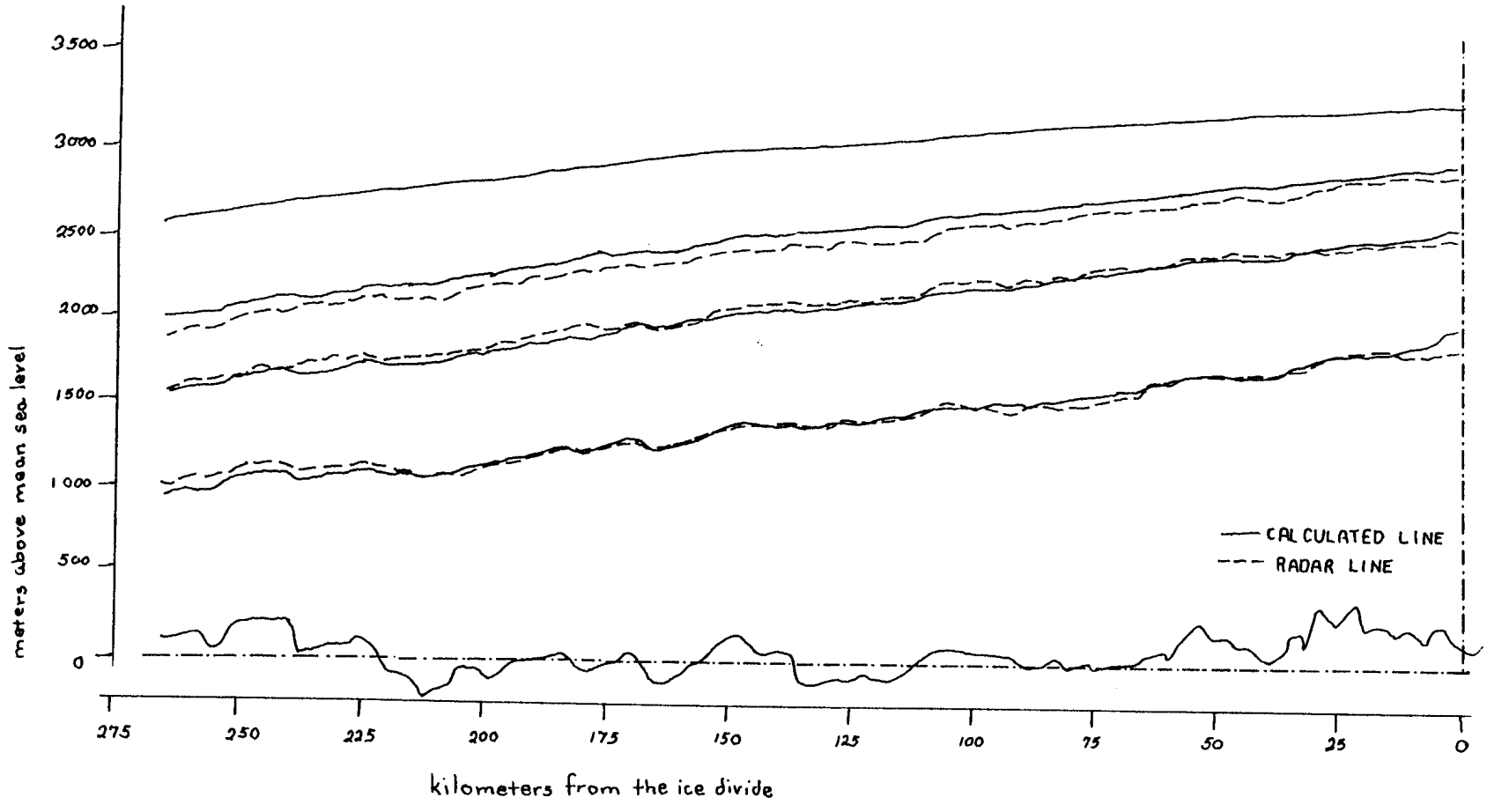
3500
3000
2500
2000
1500
1000
500
0
meters above mean sea level
CALCULATED LINE
RADAR LINE
275
250
225
200
175
150
125
100
75
50
25
0
kilometers from the ice divide

figure 12

that both thickness and accumulation have increased from 6700 years before present to the present.

Changes in thickness and accumulation are inconsistent with the steady-state assumption. It is suggested, therefore, that future investigation be directed towards developing a model which does not require this assumption. From this, deeper insight into the magnitude of changes of climatic variables, and variables internal to the ice during the past history of the Greenland ice sheet can be obtained.

SUMMARY AND CONCLUSIONS

Airborne radio echo records were obtained of a flight path that followed a flowline in the Greenland ice sheet. These records show internal layering extending over several hundred kilometers. Past investigators have suggested that these lines represent depositional surfaces.

Three widely-spaced and easy-to-follow radar lines were chosen for study. An ice flow model was used to calculate isochrons approximating the depths of these radar lines. The model assumes that there is no bottom melting or freezing, that vertical strain rates are constant with depth, and that the ice is in a steady-state.

The model was translated into a Fortran program and run on a computer. The youngest isochron agrees closely with the youngest radar line, but discrepancies occur between the older sets of radar lines and isochrons. These discrepancies increase with age and depth.

Because of the close agreement of the upper, 1400 year old lines, the assumptions in the model are considered valid for about the last 1500

years: the ice sheet has been in a close-to-steady-state, and the radar layers are indeed isochrons.

Discrepancies between the lower sets of isochrons and the radar layering may be a result of changes in the ice sheet or weaknesses in the representation of ice flow in the calculations. Errors arising from not allowing for bottom melting and freezing do not significantly affect the results. However, variance of strain rates with depth may be significant. Because the radar lines are in the upper 75% of the ice, a 20% greater "average" strain rate might be more appropriate.

Changes in thickness and accumulation rates also affect the results of the model. Using smaller values than those observed brings closer agreement to the lower two sets of isochrons. This suggests that either or both thickness and accumulation have increased from 6700 years ago to the present.

Changes in accumulation rates and in thickness cannot be incorporated into a steady-state model. Therefore, according to the model used in this study, at least part of the Greenland

ice sheet is not in a steady-state. More detailed investigation using a model which does not depend on constant strain rates with depth or on an assumption of steady-state is needed to determine the magnitude of the changes occurring in this ice sheet.

APPENDIX A: List of the Fortran computer program used in this study.

```
9 FORMAT(/' GINUT.  ICEBERGS IN GREENLAND      PROGRAM #00229')          00000020
                                                                         00000040
  REAL LAMBDA                                                            00000050
  INTEGER*4 DAISY*6,DATE
  DIMENSION BBBX(350),ELEV(350),Z(350),ADOTI(350),
 >BBAR(350),DELTAT(350),EPSILN(350),TPART(350,3),ORIGIN(350,3),
 >DEPTH(350),LAMBDA(350,3),BEDELV(350),ELVMAX(350,3),RD1400(350),
 >BB3000(350),BB4700(350),DATE(3),X(350),BDOT(350)
  DIMENSION ZZ(350)
  READ(1,700)DAISY,(BBBX(I),X(I),BDOT(I),ELEV(I),Z(I),RD6700(I),
 >BB3000(I),BB1400(I),I=1,350)
                                                                         00000100
  LAST = 347                                                             00000110
  WRITE(6,999)
  CALL PLOTS(0,0,0)
  DATE(1)=1400
  DATE(2)=3000
  DATE(3)=6700
  WRITE (6,304)
  WRITE (6,305)
  DO 11 I=1,LAST
  ZZ(I)=Z(I)
  QQ=ELEV(I)-BB3000(I)
  WRITE (6,306) I,BBBX(I),ELEV(I),BB3000(I),QQ
                                                                         00000130
  X(I)=X(I)*1000.
  BB6700(I)=ELEV(I)-BB6700(I)
  BB3000(I)=ELEV(I)-BB3000(I)
  BB1400(I)=ELEV(I)-BB1400(I)
  BEDELV(I)=ELEV(I)-ZZ(I)
                                                                         00000150
  SUM = 0.
  DO 22 I=2,LAST
                                                                         00000170
  BDOTI(I)=(BDOTA(I-1)+BDOTA(I))/2./92.                                  00000180
  SUMA = BDOTI(I)*(X(I)-X(I-1))                                          00000190
  BBAR(I)=(SUM/Z(I-1)+(SUM+SUMA)/Z(I))/2.                                00000200
  DELTAT(I)=(X(I)-X(I-1))/BBAR(I)
  EPSILN(I)=(-BDOTI(I)+BBAR(I)*(Z(I)-Z(I-1))/(X(I)-X(I-1)))/
 >((Z(I)+Z(I-1))/2.)
                                                                         00000230
2 SUM = SUM+SUMA
  DO 33 J=1,3
3 FIND SUMS OF T'S                                                       00000240
                                                                         00000260
  DO 213 L=2,LAST                                                        00000270
  SUM=0.                                                                 00000280
  M=L
  IF(DELTAT(L)-DATE(JJ)) 25,75,75
                                                                         00000300
5 SUM = SUM+DELTAT(L)                                                    00000310
  DO 33 M=1,LAST                                                         00000320
  M=L+1
  IF(SUM+DELTAT(M)-DATE(JJ))30,75,75
                                                                         00000340
30 SUM = SUM+DELTAT(M)
PART IS PARTIAL TRAVEL TIME USED IN GATE OF ORIGIN ' ORIGIN(M) -         00000350
33 TPART(L,JJ)=DATE(JJ)-SUM
33 ORIGIN(L,JJ)=1
  DO 33 I=1,LAST                                                         00000380
  M=ORIGIN(I,JJ)
  LAMBDA(M,JJ)=BDOTI(M)/(EPSILN(M)*TPART(I,JJ))*(1.-EXP(EPSILN(M)*T
 >PART(I,JJ)))
  IF(I.EQ.1) GO TO 33                                                    00000420
                                                                         00000430
  M1=M-1                                                                 00000440
  DO 33 J=M1,1
  LAMBDA(J,JJ)=BDOTI(J)/(EPSILN(J)*DELTAT(J))*(1.-EXP(EPSILN(J)*DEL
 >TAT(J)))
  JLEV=1                                                                 00000470
                                                                         00000480
  DO 33 K=1,JL
33 LAMBDA(K,JJ)=LAMBDA(K,JJ)/(EPSILN(J)*DELTAT(J))*(1.-EXP(EPSILN(J)
```

```
>*DELTAT(J)))
  DEPTH(I,JJ)=ELRADA(I,JJ)*TPAR(I,J)
    IF(I.EQ.N) GO TO 55                                                  00000520
    N=I+1                                                                00000530
    DO 55 J=N,M1                                                         00000540
  DEPTH(I,JJ)=DEPTH(I,JJ)+ELRADA(J,JJ)*DELTAT(J)
  ELVLAY(I,JJ)=ELEV(I)-DEPTH(I,JJ)
    WRITE(6,200)                                                         00000570
    I=1                                                                  00000580
    WRITE(6,202)I,OBSRVD(I),X(I),BOOTY(I),ELEV(I),REDELV(I),Z(I)         00000590
    DO 5 I=2,LAST                                                        00000600
    WRITE(6,202)BOOTY(I),ADAR(I),DELTAT(I),EPSILN(I),ORIGIN(I,JJ),TPAR
  ,I,JJ,I,DEPTH(I,JJ),ELVLAY(I,JJ)
    WRITE(6,202)I,OBSRVD(I),X(I),BOOTY(I),ELEV(I),REDELV(I),Z(I)         00000630
    WRITE (6,501)
    WRITE (6,502)
    DO 7 I=1,LAST
    WRITE (6,503) I,OBSRVD(I),BOLGOD(I),BOBSOO(I),BOB700(I)
    XSCL=10./3000.
    ELVSCL=1./1000.
AA SEA LEVEL
    CALL PLOT (0.,0.,3)
    CALL PLOT(0.,-3000.*XSCL,2)
AA BOTTOM.
    CALL PLOT (REDELV(1)*ELVSCL,-X(1)*XSCL,3)
    DO 5 I=2,LAST
    CALL PLOT (REDELV(I)*ELVSCL,-X(I)*XSCL,2)
AA SURFACE
    CALL PLOT (ELEV(1)*ELVSCL,-X(1)*XSCL,3)
    DO 9 I=2,LAST
    CALL PLOT (ELEV(I)*ELVSCL,-X(I)*XSCL,2)
AA CALCULATED LINE
    CALL PLOT (ELVLAY(2,JJ)*ELVSCL,-X(2)*XSCL,3)
    DO 8 I=3,LAST
    CALL PLOT (ELVLAY(I,JJ)*ELVSCL,-X(I)*XSCL,2)
AA MEASURED LINE
    IF (JJ.EQ.1) GO TO 29
    IF (JJ.EQ.2) GO TO 39
    CALL NEWPEN (4)
    CALL PLOT (BOB700(1)*ELVSCL,-X(1)*XSCL,3)
    WRITE (6,511)
    DO 7 I=2,LAST
    CALL PLOT(BOB700(I)*ELVSCL,-X(I)*XSCL,2)
    CALL NEWPEN (2)
    WRITE (6,512)I,OBSRVD(I),BOB700(I),ELVLAY(I,3)
    IF (BOB700(I).GT.ELVLAY(I,3)) GO TO 30
    CALL SYMBOL (ELVLAY(2,3)*ELVSCL,-X(2)*XSCL,0.07,15HCALCULATED LINE
  ,0.,15)
    CALL SYMBOL(BOB700(2)*ELVSCL-0.07,0.,0.07,10HRADAR LINE,270.,10)
    GO TO 45
    CALL SYMBOL (BOB700(I)*ELVSCL,0.,0.07,10HRADAR LINE,270.,10)
    CALL SYMBOL (ELVLAY(2,3)*ELVSCL-0.07,-X(2)*XSCL,0.07,15HCALCULATED
  LINE,270.,15)
    GO TO 45
    CALL NEWPEN (4)
    CALL PLOT(BOL400(1)*ELVSCL,-X(1)*XSCL,3)
    WRITE (6,511)
    DO 42 I=2,LAST
    WRITE (6,512)I,OBSRVD(I),BOL400(I),ELVLAY(I,1)
    CALL PLOT (BOL400(I)*ELVSCL,-X(I)*XSCL,2)
    CALL NEWPEN (2)
    IF (BOL400(I).GT.ELVLAY(2,1)) GO TO 208
```

```
      CALL SYMBOL (ELVLAY(2,1)*ELVSCL,-X(2)*XSCL,0.07,15HCALCULATED LINE
     ,,270.,15)
      CALL SYMBOL (DDJ+DD(1)*ELVSCL-0.07,0.,0.07,10HRADAR LINE,270.,10)
      GO TO 45
   CALL SYMBOL (DDJ+DD(1)*ELVSCL,0.,0.07,10HRADAR LINE,270.,10)
      CALL SYMBOL (ELVLAY(2,1)*ELVSCL-0.07,-X(2)*XSCL,0.07,15HCALCULATED
     , LINE,270.,15)
      GO TO 45
   CALL PLOT (DDJDD(1)*ELVSCL,-X(1)*XSCL,3)
      WRITE (6,211)
      DO 44 I=2,LAST
      WRITE (6,212)I,DDJDD(I),DDJDD(I),FLVLAY(I,2)
      CALL PLOT (DDJDD(I)*ELVSCL,-X(I)*XSCL,2)
      CALL NEWPEN (1)
      IF (DDJDD(I).GT.ELVLAY(2,2)) GO TO 207
      CALL SYMBOL (ELVLAY(2,2)*ELVSCL,-X(2)*XSCL,0.07,15HCALCULATED LINE
     ,,270.,15)
      CALL SYMBOL(DDJDD(I)*ELVSCL-0.07,0.,0.07,10HRADAR LINE,270.,10)
      GO TO 45
   CALL SYMBOL (DDJDD(I)*ELVSCL,0.,0.07,10HRADAR LINE,270.,10)
      CALL SYMBOL (ELVLAY(2,2)*ELVSCL-0.07,-X(2)*XSCL,0.07,15HCALCULATED
     , LINE,270.,15)
   CONTINUE
      CALL PLOT (-250.*ELVSCL,-250000.*XSCL,3)
      CALL PLOT (-250.*ELVSCL,0.,2)
      NSUM=0
      DO 200 KK=1,15
      CALL SYMBOL (-250.*ELVSCL,-NSUM*XSCL,0.14,-3,0.,-1)
   NSUM=NSUM+25000
      CALL PLOT (-250.*ELVSCL,-250000.*XSCL,3)
      CALL PLOT (250.*ELVSCL,-250000.*XSCL,2)
      NKSUM=0
      DO 194 KKK=1,6
      CALL SYMBOL (NKSUM*ELVSCL,-300000.*XSCL,0.14,-3,0.,-1)
   NKSUM=NKSUM+50000
   CONTINUE
      CALL PLOT (0.,0.,,999)
      STOP                                                    00000640
```

APPENDIX B: Table of data showing latitude, longitude, distance from the ice divide, and accumulation data for each CBD no. along the flowline.

CBD NO.	LONGITUDE	LATITUDE	DISTANCE FROM ICE DIVIDE (m.)	ACCUMULATION ($m.H_2O$)
270	-37.282	71.115	0	0.27
269	-37.350	71.113	2000	0.27
268	-37.412	71.112	4000	0.27
267	-37.465	71.105	6000	0.28
266	-37.523	71.102	8000	0.28
265	-37.572	71.098	10000	0.28
264	-37.633	71.092	12000	0.28
263	-37.690	71.088	14000	0.28
262	-37.738	71.083	16000	0.28
261	-37.800	71.082	18000	0.28
260	-37.852	71.080	20000	0.28
259	-37.920	71.078	22000	0.28
258	-37.978	71.077	24000	0.29
257	-38.025	71.077	26000	0.29
256	-38.092	71.072	28000	0.29
255	-38.137	71.072	30000	0.29
254	-38.203	71.070	32000	0.29
253	-38.265	71.068	34000	0.29
252	-38.315	71.065	36000	0.29
251	-38.377	71.060	37000	0.29
250	-38.423	71.055	39000	0.29
249	-38.482	71.048	40000	0.29
248	-38.540	71.043	42000	0.29
247	-38.577	71.037	44000	0.30
246	-38.637	71.027	46000	0.30
245	-38.683	71.020	48000	0.30
244	-38.735	71.013	50000	0.30
243	-38.795	71.008	52000	0.30
242	-38.910	71.003	55000	0.30
241	-38.997	71.003	58000	0.31
240	-39.015	71.003	62000	0.31
239	-39.082	71.003	64000	0.31
238	-39.140	71.000	65000	0.32
237	-39.200	70.997	69000	0.32
236	-39.240	70.990	70000	0.32
235	-39.303	70.987	72000	0.32
234	-39.362	70.985	74000	0.32
233	-39.412	70.980	76000	0.32
232	-39.473	70.980	78000	0.33
231	-39.525	70.980	81000	0.33

CBD NO.	LONGITUDE	LATITUDE	DISTANCE FROM ICE DIVIDE (m.)	ACCUMULATION ($m.H_2O$)
230	-39.588	70.978	83000	0.33
229	-39.648	70.977	84000	0.33
228	-39.702	70.977	85000	0.33
227	-39.763	70.975	87000	0.33
226	-39.810	70.975	88000	0.34
225	-39.873	70.973	89000	0.34
224	-39.932	70.967	90000	0.34
223	-39.982	70.963	91000	0.34
222	-40.042	70.955	92000	0.34
221	-40.090	70.952	93000	0.34
220	-40.145	70.945	94000	0.34
219	-40.203	70.942	97000	0.35
218	-40.248	70.940	100000	0.35
217	-40.313	70.938	103000	0.35
216	-40.367	70.935	109000	0.35
215	-40.430	70.935	112000	0.36
214	-40.490	70.935	115000	0.36
213	-40.533	70.933	118000	0.36
212	-40.602	70.932	121000	0.36
211	-40.648	70.928	124000	0.37
210	-40.688	70.913	126000	0.37
209	-40.728	70.902	128000	0.37
208	-40.762	70.890	130000	0.37
207	-40.815	70.878	132000	0.37
206	-40.868	70.875	134000	0.38
205	-40.910	70.867	136000	0.38
204	-40.965	70.862	138000	0.38
203	-41.012	70.855	140000	0.38
202	-41.068	70.850	141000	0.38
201	-41.118	70.840	143000	0.38
200	-41.162	70.832	144000	0.38
199	-41.208	70.820	147000	0.38
198	-41.250	70.813	150000	0.39
197	-41.298	70.803	152000	0.39
196	-41.355	70.797	155000	0.39
195	-41.355	70.792	158000	0.39
194	-41.463	70.787	160000	0.40
193	-41.513	70.783	161000	0.40
192	-41.617	70.768	163000	0.40
191	-41.650	70.758	166000	0.40

CBD NO.	LONGITUDE	LATITUDE	DISTANCE FROM ICE DIVIDE (m.)	ACCUMULATION ($m.H_2O$)
190	-41.695	70.743	168000	0.41
189	-41.727	70.737	170000	0.41
188	-41.770	70.727	172000	0.41
187	-41.820	70.717	174000	0.41
186	-41.875	70.713	176000	0.41
185	-41.933	70.708	178000	0.42
184	-41.977	70.705	180000	0.42
183	-42.037	70.703	182000	0.42
182	-42.090	70.697	184000	0.42
181	-42.135	70.692	186000	0.42
180	-42.185	70.683	187000	0.42
179	-42.232	70.675	189000	0.42
178	-42.283	70.667	190000	0.43
177	-42.338	70.660	192000	0.43
176	-42.383	70.655	194000	0.43
175	-42.440	70.648	197000	0.43
174	-42.482	70.645	200000	0.43
173	-42.537	70.638	202000	0.43
172	-42.590	70.628	203000	0.44
171	-42.633	70.622	205000	0.44
170	-42.680	70.610	206000	0.44
169	-42.713	70.602	208000	0.44
168	-42.760	70.590	210000	0.44
167	-42.805	70.582	212000	0.44
166	-42.852	70.575	214000	0.45
165	-42.907	70.568	216000	0.45
164	-42.953	70.565	218000	0.45
163	-43.008	70.557	220000	0.45
162	-43.065	70.553	224000	0.45
161	-43.110	70.547	225000	0.45
160	-43.160	70.537	226000	0.45
159	-43.197	70.532	228000	0.45
158	-43.243	70.518	230000	0.45
157	-43.288	70.507	232000	0.45
156	-43.330	70.497	234000	0.46
155	-43.383	70.488	236000	0.46
154	-43.422	70.485	238000	0.46
153	-43.478	70.480	240000	0.46
152	-43.535	70.477	242000	0.46
151	-43.582	70.475	244000	0.46
150	-43.637	70.467	245000	0.46

CBD NO.	LONGITUDE	LATITUDE	DISTANCE FROM ICE DIVIDE (m.)	ACCUMULATION ($m.H_2O$)
149	-43.673	70.458	247000	0.47
148	-43.728	70.450	250000	0.47
147	-43.783	70.440	252000	0.47
146	-43.817	70.433	254000	0.48
145	-43.865	70.422	256000	0.48
144	-43.907	70.417	258000	0.48
143	-43.957	70.408	260000	0.48
142	-44.045	70.388	262000	0.49
141	-44.087	70.377	264000	0.49
140	-44.122	70.367	266000	0.49
139	-44.168	70.357	268000	0.49
138	-44.220	70.348	270000	0.50

APPENDIX C: Table of data showing surface and substrate elevations and ice thickness for each CBD no. along the flowline.

CBD NO.	SURFACE ELEV. (m.)	SUBSTRATE ELEV. (m.)	ICE THICKNESS (m.)
270	3263	153	3110
269	3262	112	3150
268	3262	132	3130
267	3258	158	3100
266	3257	257	3000
265	3251	251	3000
264	3250	150	3100
263	3249	219	3030
262	3244	244	3000
261	3245	195	3050
260	3243	243	3000
259	3232	252	2980
258	3229	219	3010
257	3225	375	2850
256	3219	329	2890
255	3225	245	2980
254	3219	319	2900
253	3213	363	2850
252	3211	111	3100
251	3206	206	3000
250	3202	202	3000
249	3197	97	3100
248	3183	63	3120
247	3182	32	3150
246	3185	85	3100
245	3178	128	3050
244	3174	124	3050
243	3180	180	3000
242	3163	163	3000
241	3160	260	2900
240	3153	153	3000
239	3144	44	3100
238	3145	95	3050
237	3143	63	3080
236	3130	20	3110
235	3130	20	3110
234	3128	28	3100
233	3123	23	3100
232	3115	-5	3120
231	3112	22	3090

CBD NO.	SURFACE ELEV. (m.)	SUBSTRATE ELEV. (m.)	ICE THICKNESS (m.)
230	3104	4	3100
229	3097	-13	3110
228	3096	-4	3100
227	3090	40	3050
226	3091	21	3070
225	3087	7	3080
224	3077	-3	3080
223	3073	-7	3080
222	3069	-11	3080
221	3065	-15	3080
220	3071	11	3060
219	3057	57	3000
218	3055	55	3000
217	3052	62	2990
216	3044	94	2950
215	3035	85	2950
214	3024	24	3000
213	3012	-38	3050
212	3007	-93	3100
211	3012	-88	3100
210	2998	-52	3050
209	2998	-102	3100
208	3000	-100	3100
207	2997	-83	3080
206	2981	-99	3080
205	2980	-120	3100
204	2977	-113	3090
203	2975	-95	3070
202	2967	37	2930
201	2961	71	2890
200	2954	74	2880
199	2951	51	2900
198	2949	119	2830
197	2944	164	2780
196	2930	120	2810
195	2930	20	2910
194	2918	-12	2930
193	2911	-9	2920
192	2895	-65	2960
191	2889	-111	3000

CBD NO.	SURFACE ELEV. (m.)	SUBSTRATE ELEV. (m.)	ICE THICKNESS (m.)
190	2879	-141	3020
189	2873	-107	2980
188	2881	-9	2890
187	2879	49	2830
186	2867	-3	2870
185	2865	-15	2880
184	2857	-23	2880
183	2842	-58	2900
182	2833	-47	2880
181	2831	-19	2850
180	2826	36	2790
179	2816	36	2780
178	2813	13	2800
177	2812	12	2800
176	2802	2	2800
175	2788	-12	2800
174	2786	-64	2850
173	2779	-111	2890
172	2773	-117	2890
171	2762	-48	2810
170	2754	-56	2810
169	2749	-41	2790
168	2741	-159	2900
167	2737	-163	2900
166	2730	-180	2910
165	2720	-230	2950
164	2721	-149	2870
163	2714	-96	2810
162	2704	-86	2790
161	2698	-12	2710
160	2692	22	2670
159	2687	87	2600
158	2676	126	2550
157	2672	62	2610
156	2668	58	2610
155	2652	82	2570
154	2644	54	2590
153	2641	41	2600
152	2633	23	2610
151	2625	235	2390

CBD NO.	SURFACE ELEV. (m.)	SUBSTRATE ELEV. (m.)	ICE THICKNESS (m.)
150	2619	219	2400
149	2615	215	2400
148	2602	212	2390
147	2593	213	2380
146	2588	208	2380
145	2576	166	2410
144	2561	71	2490
143	2552	62	2490
142	2538	138	2400
141	2535	145	2390
140	2527	127	2400
139	2513	103	2410
138	2510	120	2390

APPENDIX D: Table of data showing measured elevations (in meters) for the radar lines chosen for study. Measurements are given for each CBD no. along the flowline. Numbers given in heading of radar lines indicate ages used in calculation of comparable isochrons (in years.)

CBD NO.	ELEV. OF RADAR LINE 1400	ELEV. OF RADAR LINE 3050	ELEV. OF RADAR LINE 6700
270	2833	2473	1863
269	2842	2462	1842
268	2842	2462	1842
267	2848	2458	1838
266	2837	2477	1837
265	2831	2461	1831
264	2830	2440	1790
263	2839	2449	1799
262	2834	2444	1794
261	2835	2445	1805
260	2833	2443	1823
259	2812	2422	1812
258	2819	2429	1819
257	2805	2425	1815
256	2809	2409	1809
255	2805	2405	1805
254	2769	2389	1789
253	2763	2403	1763
252	2751	2421	1731
251	2726	2416	1716
250	2722	2402	1722
249	2707	2407	1707
248	2693	2383	1683
247	2682	2372	1672
246	2705	2375	1685
245	2698	2368	1668
244	2714	2384	1684
243	2710	2390	1680
242	2683	2363	1683
241	2680	2360	1670
240	2663	2353	1653
239	2644	2324	1644
238	2635	2315	1635
237	2633	2303	1623
236	2630	2280	1570
235	2630	2280	1550
234	2618	2298	1548
233	2623	2283	1533
232	2605	2285	1525
231	2612	2272	1502

CBD NO.	ELEV. OF RADAR LINE 1400	ELEV. OF RADAR LINE 3050	ELEV. OF RADAR LINE 6700
230	2594	2244	1484
229	2587	2217	1497
228	2586	2226	1486
227	2570	2240	1480
226	2571	2241	1481
225	2557	2217	1497
224	2547	2207	1497
223	2553	2213	1493
222	2549	2219	1499
221	2545	2215	1475
220	2551	2211	1481
219	2527	2177	1457
218	2545	2185	1475
217	2522	2202	1472
216	2504	2194	1494
215	2485	2185	1485
214	2444	2114	1434
213	2432	2112	1412
212	2417	2097	1397
211	2422	2092	1392
210	2408	2068	1378
209	2418	2078	1388
208	2420	2090	1390
207	2417	2067	1387
206	2391	2061	1361
205	2400	2060	1360
204	2397	2057	1357
203	2405	2065	1365
202	2407	2067	1377
201	2411	2061	1361
200	2374	2054	1354
199	2371	2051	1371
198	2369	2049	1349
197	2364	2034	1354
196	2350	2020	1330
195	2340	2000	1310
194	2328	1958	1298
193	2311	1961	1291
192	2295	1935	1265
191	2289	1909	1239

CBD NO.	ELEV. OF RADAR LINE 1400	ELEV. OF RADAR LINE 3050	ELEV. OF RADAR LINE 6700
190	2279	1899	1229
189	2273	1893	1213
188	2271	1931	1231
187	2279	1929	1239
186	2267	1917	1247
185	2265	1895	1225
184	2257	1897	1227
183	2232	1912	1212
182	2233	1913	1203
181	2231	1911	1211
180	2226	1906	1216
179	2216	1876	1206
178	2213	1873	1203
177	2202	1862	1182
176	2202	1852	1172
175	2158	1818	1128
174	2166	1816	1116
173	2159	1799	1109
172	2153	1783	1103
171	2152	1772	1092
170	2144	1764	1074
169	2129	1759	1059
168	2091	1741	1051
167	2067	1737	1057
166	2060	1730	1050
165	2080	1720	1040
164	2071	1721	1051
163	2064	1714	1064
162	2064	1714	1084
161	2098	1698	1098
160	2082	1712	1102
159	2087	1737	1127
158	2056	1746	1116
157	2042	1712	1092
156	2038	1718	1088
155	2042	1702	1092
154	2024	1694	1084
153	2031	1701	1081
152	2023	1673	1073
151	2005	1665	1105

CBD NO.	ELEV. OF RADAR LINE 1400	ELEV. OF RADAR LINE 3050	ELEV. OF RADAR LINE 6700
150	1979	1659	1099
149	1995	1655	1125
148	1982	1662	1112
147	1963	1623	1103
146	1958	1608	1098
145	1936	1606	1056
144	1911	1591	1051
143	1892	1582	1032
142	1898	1568	1038
141	1885	1585	1025
140	1877	1557	1017
139	1853	1533	983
138	1830	1520	990

REFERENCES CITED

Benson, C.S. 1962. Stratigraphic Studies in the Snow and Firn of the Greenland Ice Sheet. U.S. Army Snow, Ice and Permafrost Research Establishment. Research Report 70, p. 13-42.

Clough, J.W. 1977. Radio-echo sounding: reflection from internal layers in ice sheets. Journal of Glaciology, vol. 18, no. 78, p. 3-13.

Harrison, C.H. 1973. Radio echo sounding of horizontal layers in ice. Journal of Glaciology, vol. 12, no. 66, p. 383-97.

Paterson, W.S.B. 1969. The Physics of Glaciers. Oxford. Pergamon Press, 233 p.

Robin, G. de Q. 1969. Radio echo sounding in polar ice sheets by G. de Q. Robin, S. Evans and J.T. Baily. Philosophical Transactions of the Royal Society of London, vol. 265, no. 1166, p. 437-505.

Weidick, A. 1975. A Review of Quaternary Investigations in Greenland. Institute of Polar Studies. Report no. 55. Ohio State University. 161 p.

Whillans, I.M. 1976. Radio-echo layers and the recent stability of the West Antarctic ice sheet. Nature, vol. 264, no. 5582, p. 152-55.